Supporting Information Available:

Photoresponsive and Gas Sensing Field-Effect Transistors based on Multilayer WS_2 Nanoflakes

Nengjie Huo[1], Shengxue Yang[1], Zhongming Wei[2], Shu-Shen Li[1], Jian-Bai Xia[1] & Jingbo Li[1*]

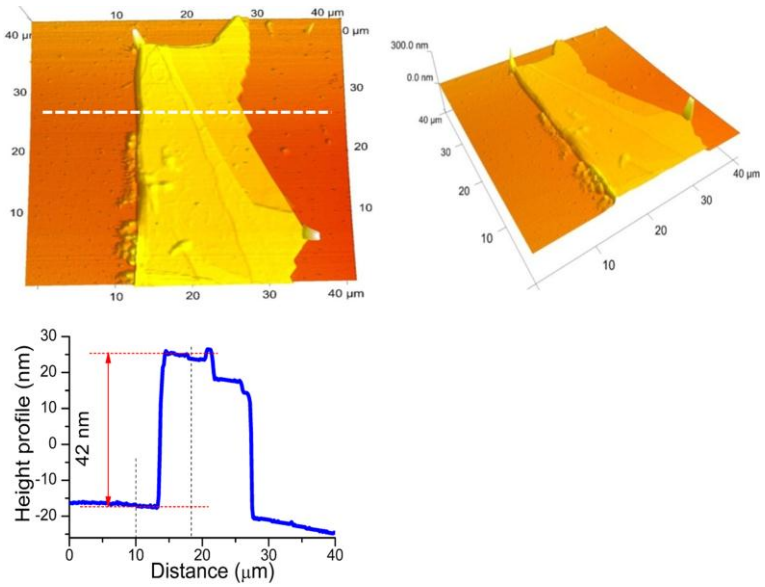

Figure S1 Atomic force microscopy (AFM) images of the actual device based on multilayer WS_2 nanoflakes, cross-sectional plot along the line determines the thickness of WS_2 nanoflakes to be 42 nm.

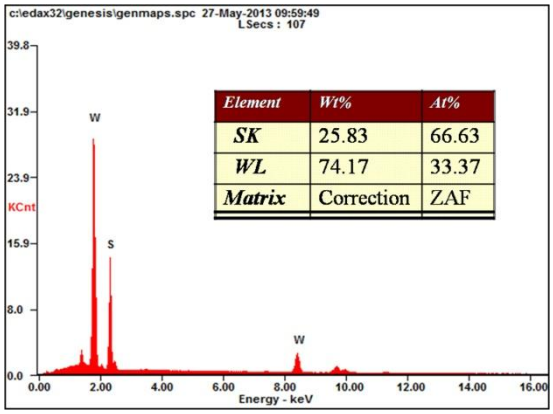

Figure S2 Energy Dispersive X-ray Spectra (EDX) of the multilayer WS_2 nanoflakes. The inset corresponds to the weight and atoms percentages, indicating the existence of S/W elements with an atom ratio of 2.

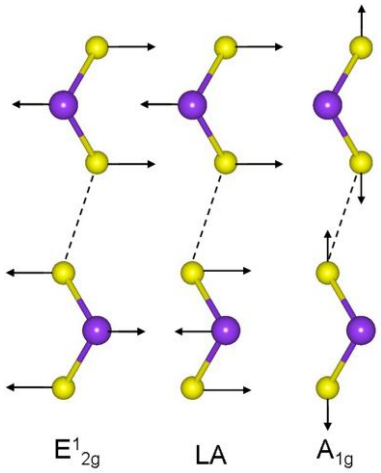

Figure S3 Schematic diagram of Raman modes of WS_2 nanosheets. LA (M) is in-plane collective movements of the atoms in the lattice, $E^1_{2g}(\Gamma)$ is an in-plane optical mode, and $A_{1g}(\Gamma)$ corresponds to out-of-plane vibrations of the sulfur atoms. The dashed line represents the weak inter-layer van der waals interaction.

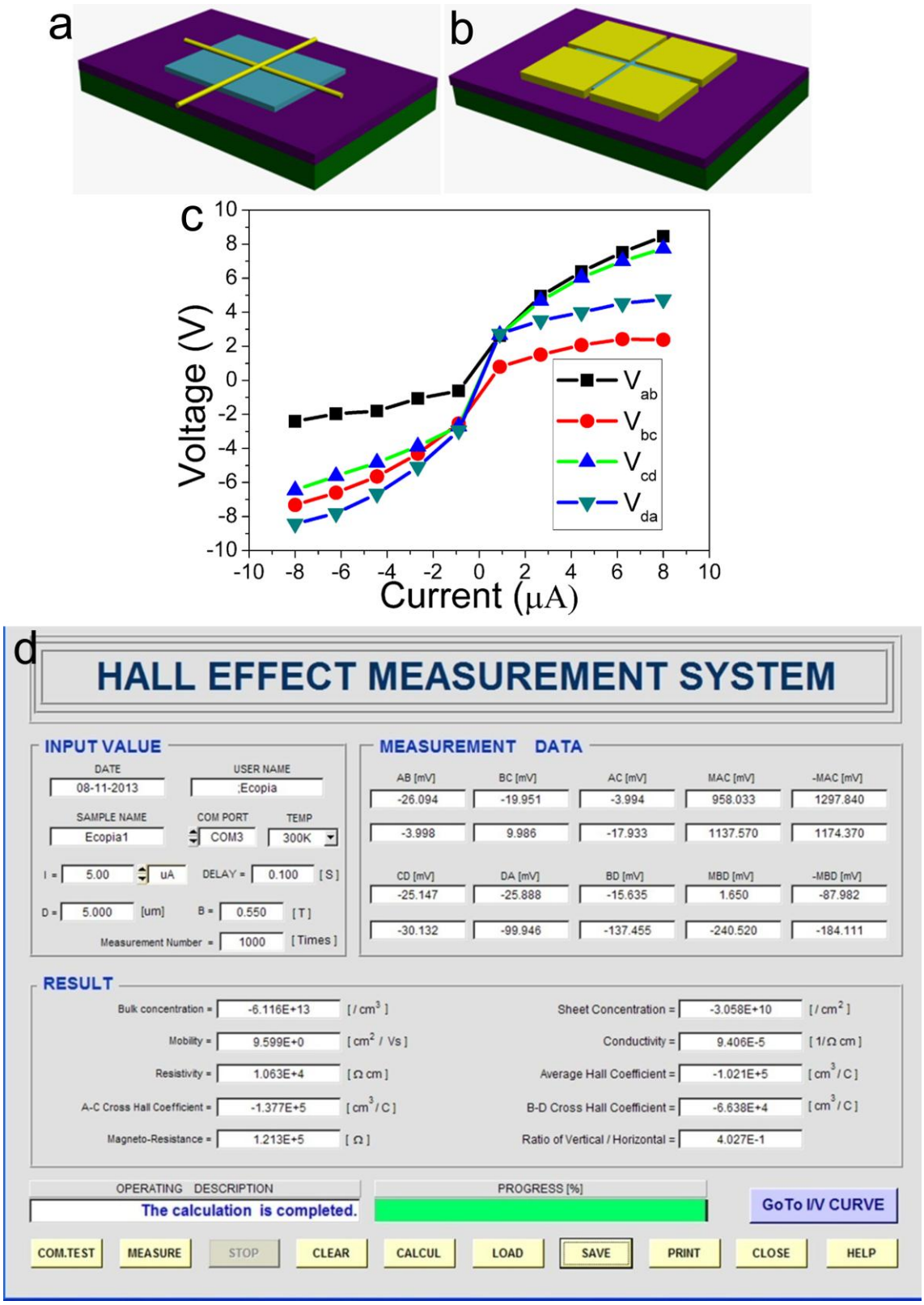

Figure S4 (a,b) Schematic diagram of the four-electrode device fabrication for Hall measurements. (c) I-V curves of four contacts indicating the successful contact of four

electrodes on the WS_2 nanoflaks. (d) Final Hall results of the multilayer WS_2 nanoflakes measured with four-probes at room temperature, performing an n-type behavior with mobility (μ) of 9.6 cm^2/Vs.

The detailed process: Firstly, the four-electrode device was fabricated with "gold-wire mask moving" technique as shown in Figure S4a and b. Secondly, the device was connected with four probes equipped on Hall Effect Measurement System (HMS-300), then measured I-V curves to ensure the successful contact of the four electrodes (Figure S4c shows the successful contact of four electrode on WS_2 nanoflakes). Then, enter the Hall measurement, and switch the magnetic (0.55 T) direction from $N \rightarrow S$ and $S \rightarrow N$, respectively. Finally, the system can automatically output the electrical parameters of the device directly including the Mobility and sheet concentration as shown in Figure S4d.

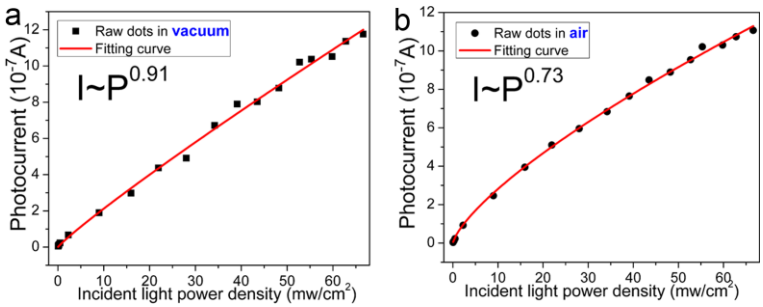

Figure S5 Photocurrent (defined as $I_{ph} = I_{light} - I_{dark}$) as function of illumination density in vacuum (a) and air (b). All curves were measured at V_{DS}= 1 V. A 633 nm laser was used to excite the photocurrent.

The reason for higher (or lower) gas sensitivity of ethanol and NH_3 (or

O_2) measured under light compared to under dark:

Based on the discussions in text, large amounts of O_2 and air molecules are adsorbed under light illumination due to that the redundant photo-excited electrons need more oxidizing gas like O_2 to be accepted, but very poorly O_2 molecules are adsorbed in dark due to the less electrons. Thus, the gas sensitivity in light is larger than that in dark for O_2 and air. For the reducing gas like NH_3 and ethanol, substantial gas molecules have been adsorbed in dark, leading to high gas sensitivity in dark. In the presence of light, abundant photo-excited electrons have existed in the device, although the photo-generated holes will attract more reducing gas like NH_3 and ethanol to be adsorbed, the proportion of increased electron caused by adsorbed donors is still little among the total amounts of electrons, resulting in the lower gas sensitivity in light.

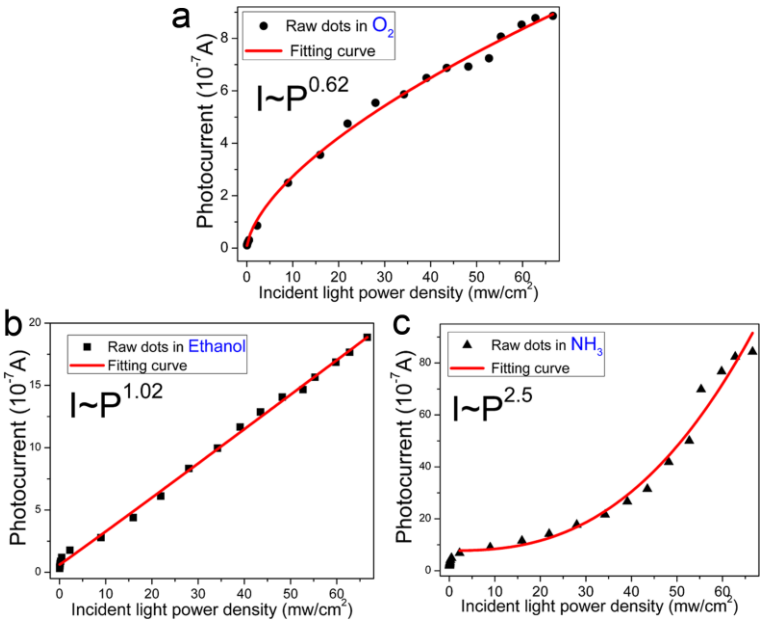

Figure S6 Photocurrent of the WS_2 nanoflakes based device for different light illumination power densities under (a) O_2, (b) ethanol, and (c) NH_3.

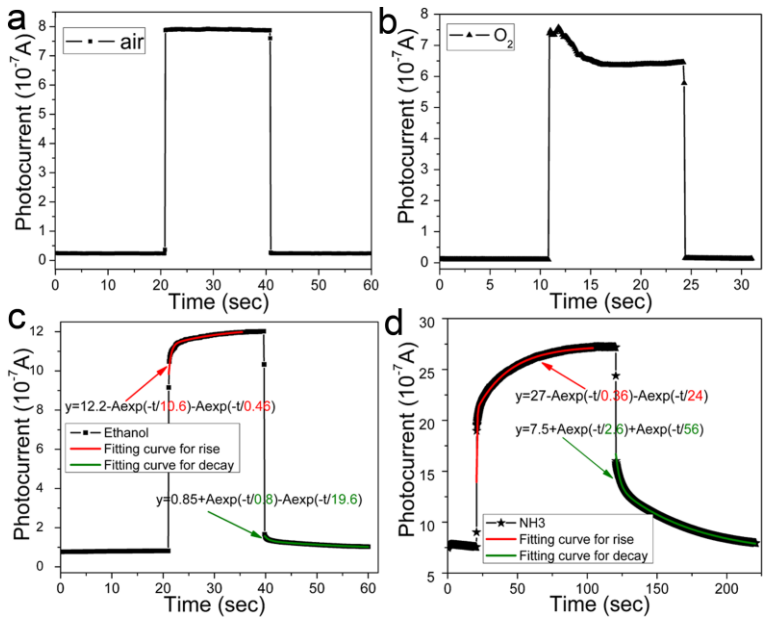

Figure S7 Dynamic response to the light illumination (633 nm, 40 mW/cm^2) under different gas atmospheres: (a) air, (b) O_2, (c) ethanol and (d) NH_3. The experimental data in ethanol and NH_3 for rise and fall are fitted by double exponential formula $I(t) = y_0 + A_1 \exp(-\frac{\tau_1}{t}) + A_2 \exp(-\frac{\tau_2}{t})$, indicating the existence of two physical mechanisms in the dynamic response process including light illumination and gas adsorption effect.

The presence of gas molecules can affect the dynamic response of the device. According to the discussion in text, the rise time τ_r and decay time τ_d in air under light illumination are both less than 20 ms (Figure S7a). When the device is exposed into the O_2 atmosphere, the rise and decay time are unchanged, but the photocurrent reaches maximum instantly upon light illumination, and then decreases into a steady photocurrent by relatively slow process of 5 s shown in Figure S7b. The subsequently decrease process of photocurrent can be attributed to that more O_2 molecules will be further adsorbed and more electrons are slowly transferred into the O_2 molecules from

the multilayer WS_2 nanoflakes when the light is switched on. Figure S7c and S7d show the response properties of the device under ethanol and NH_3 atmosphere respectively, displaying rapid rise and then slow increase process into saturation photocurrent when the light is switched on, following, quickly drop and subsequently slow decrease process into the initial dark current when the light is switched off. We consider the rise and fall photocurrent as two physical processes, one is the rapid generation or recombination of photo-excited electron-hole pairs and another is gas adsorption and charge transfer process. Unlike the single exponential formula for fitting the rise and fall time, in our device the dynamic response for rise and fall under the reducing atmosphere (ethanol and NH_3) can be perfectly fitted by double exponential formula: $I(t) = I_{photo} - A_1 \exp(-\frac{\tau_r}{t}) - A_2 \exp(-\frac{\tau_r'}{t})$ and $I(t) = I_{dark} + A_1 \exp(-\frac{\tau_d}{t}) + A_2 \exp(-\frac{\tau_d'}{t})$, where I_{photo} is saturation photocurrent; I_{dark} is initial dark current; A is a scaling constant; τ_r and τ_d are considered as rise and decay time respectively from generation or recombination of photo-excited electron-hole pairs; τ_r' and τ_d' are rise and decay time respectively from charge transfer between adsorbed gas molecules and the device. The fitting results are shown in the insert of Figure S7c and S7d, indicating the existence of two physical mechanisms in the dynamic response process to the light illumination. When the light is switched on, the electron-hole pairs are generated and extracted quickly by external voltage, forming the rapid increased photocurrent with rise time τ_r of 0.46 s in ethanol (0.36 s in NH_3), and then the further adsorbed ethanol or NH_3 molecules donate the electrons into the device slowly, leading to the slow increased current with rise time τ_r' of 10.6 s in ethanol (24 s in NH_3). For the same reason, when

the light is switched off, the recombination process of electron-hole pairs is fast, leading to the quick drop current with fall time τ_d of 0.8 s in ethanol (2.6 s in NH_3), and subsequently, the adsorbed ethanol or NH_3 molecules in the surface of the multilayer WS_2 nanoflakes will be desorbed slowly and take away the electrons in the device, resulting in the slow decreased current with decay time of τ_d' of 20 s in ethanol (56 s in NH_3).

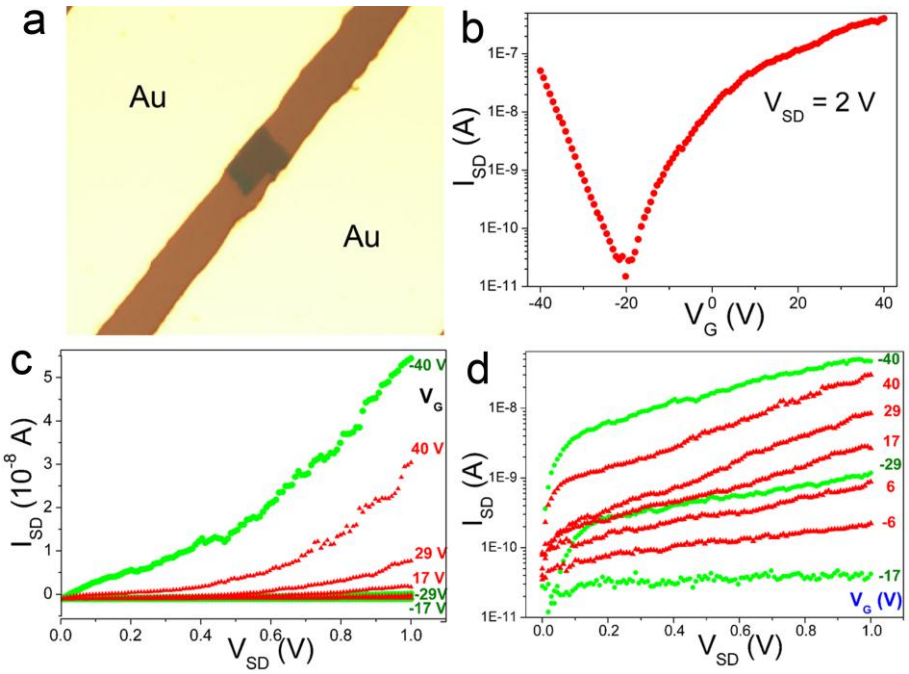

Figure S8 (a) The optical microcopy image of the few-layer (2-3) WS_2 based transistors. (b) The transfer characteristics of the device, exhibiting ambipolar properties with on/off ratio $>10^4$. The output characteristics of the device on a linear scale (c) and log scale (d) of y-axis, showing the typical ambipolar characters of the device.

Table S1 The comparisons of the optoelectronic parameters between the WS_2 nanoflakes in this work and other 2D materials in previous reports.

Parameters	R_λ (A/W)	EQE (%)	Response time	Conductive type	Mobility (cm^2/Vs)	References
GaSe nanosheet	2.8	1367 %	20 ms-7 s	p-type	0.6	[S1, S2]
GaS nanosheet	4.2	2050 %	30 ms	n-type	0.1	[S2, S3]
Single layer MoS_2	7.5×10^{-3}	--	50 ms	n-type	0.03-0.23	[S4, S5]
Few-layer MoS_2	0.57	--	70-110 μs	n-type	0.1-10	[S6-S8]
WS_2 nanotubes	4.2	615 %	245 μs	--	--	[S9]
CVD WS_2 monolayer	--	--	--	n-type	0.01	[S7]
Graphene oxide	4×10^{-3}	0.3 %	2 s	--	--	[S10]
graphene	1×10^{-3}	6-16 %	~ ps	ambipolar	1,5000	[S11,S12]
WS_2 nanoflakes	884	1.7 $\times 10^5$ %	< 20 ms	n-type	12	This work

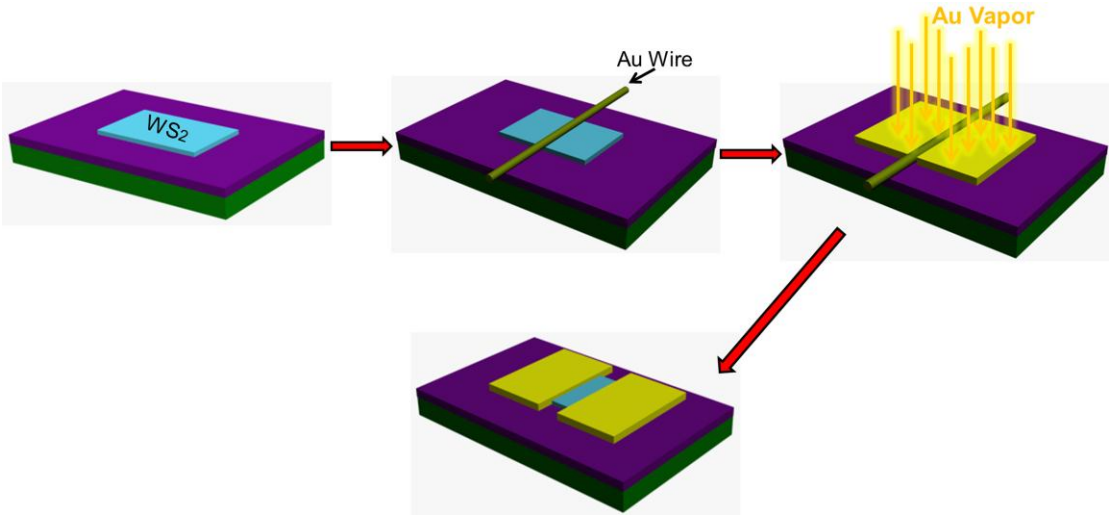

Figure S9 Schematic diagram of "gold-wire mask moving" technique for the fabrication of WS_2 nanoflakes transistors.

Preparation of WS_2 nanoflakes with mechanical exfoliation technique:

1. The WS_2 crystals slice purchased from Lamellae Co. are pasted on magnetic adhesive tape.

2. Folding the sticky side of the tape in half then tearing the tape very slowly, thus the WS_2 slices are divided into two.

3. Repeating this operation for many times until very thin nanoflakes are exfoliated on the tape.

4. Exfoliating the WS_2 nanoflakes onto SiO_2/Si substrate by pressing the tape gently and then remove it slowly.

Characterization

The images and thickness of the multilayer WS_2 nanoflakes based transistors were detected with scanning electron microscopy (SEM) and Atomic force microscopy (AFM). The energy-dispersive spectrum is measured by energy-dispersive X-ray spectroscopy (EDX) equipped on the SEM instrument. The Raman spectra were measured from 100-800 cm^{-1} using the 532 nm wavelength of a He-Ne laser. Field-effect properties were measured with Transistor test system (Agilent-B2902). Photoelectrical experiments were performed with a CHI660D electrochemical workstation in a conventional three-electrode electrochemical cell. Hall measurements were performed in Hall Effect Measurement System (HMS-300) with four probes method.

References

S1. Hu, P. A. *et al*. Synthesis of Few-Layer GaSe Nanosheets for High Performance Photodetectors. *ACS Nano* **6,** 5988-5994 (2012).

S2. Dattatray, J. L. *et al*. GaS and GaSe Ultrathin Layer Transistors. *Adv. Mater*. **24,** 3549-3554 (2012).

S3. Hu, P. A. *et al*. Highly Responsive Ultrathin GaS Nanosheet Photodetectors on Rigid and Flexible Substrates. *Nano Lett.* **13,** 1649-1654 (2013).

S4. Yin, Z. *et al.* Single Layer MoS_2 Photodetectors. *ACS Nano* **6,** 74-80 (2012).

S5. Zhang, W. *et al*. High-Gain Phototransistors Based on a CVD MoS_2 Monolayer. *Adv. Mater*. **25,** 3456-3461 (2013).

S6. Tsai, D. S. *et al*. Few-Layer MoS_2 with High Broadband Photogain and Fast Optical Switching for Use in Harsh Environments. *ACS Nano* **7,** 3905-3911 (2013).

S7. Lee, Y. H. *et al*. Synthesis and Transfer of Single-Layer Transition Metal Disulfides on Diverse Surfaces. *Nano Lett*. **13,** 1852-1857 (2013).

S8. Novoselov, K. S. *et al.* Two-dimensional atomic crystals. *Proc. Natl Acad. Sci. USA* **102,** 10451-10453 (2005).

S9. Zhang, C. *et al.* High-performance photodetectors for visible and near-infrared lights based on individual WS_2 nanotubes. *Appl. Phys. Lett*. **100,** 243101 (2012).

S10. Chitara, B., Panchakarla, L. S., Krupanidhi, S. B. & Rao, C. N. R. Infrared Photodetectors Based on Reduced Graphene Oxide and Graphene Nanoribbons. *Adv. Mater.* **23,** 5419-5423 (2011).

S11. Xia, F., Thomas, M., Lin, Y., Valdes-Garcia, A. & Avouris, P. Ultrafast Graphene Photodetector. *Nat. Nanotechnol*. **4,** 839 (2009).

S12. Geim, A. K. & Novoselov, K. S. The rise of graphene. *Nature Mater.* **6,** 183-191 (2007).